Available online at www.sciencedirect.com
SCIENCE DIRECT®
Journal of Power Sources 136 (2004) 80–87
JOURNAL OF POWER SOURCES
www.elsevier.com/locate/jpowsour

Cu_3P as anode material for lithium ion battery: powder morphology and electrochemical performances☆

Marie-Pierre Bichat[a], Tatiana Politova[a], Heriberto Pfeiffer[b], Franck Tancret[b], Laure Monconduit[a], Jean-Louis Pascal[a], Thierry Brousse[b], Frédéric Favier[a,*]

[a] *Laboratoire des Agrégats Moléculaires et Matériaux Inorganiques, UMR 5072 CNRS Université Montpellier 2, F 34095 Montpellier Cedex 05, France*
[b] *Laboratoire de Génie des Matériaux, Ecole Polytechnique de l'Université de Nantes, BP50609, 44306 Nantes Cedex 3, France*

Received 9 January 2004; accepted 3 May 2004

Available online 17 July 2004

Abstract

Cu_3P is studied as a potential material to be used as anode in a Li-ion battery. Depending on the synthetic route, solvothermal, ball-milling (with or without annealing), spray method or ceramic, used for its preparation, Cu_3P shows various particle sizes and crystallinities. The electrochemical reactivity towards lithium of these various Cu_3P powders is discussed through galvanostatic and potentiodynamic measurements, electron microscopy techniques, and X-ray diffraction on powder. Electrochemical performances, especially initial capacity and capacity retention, are shown to strongly correlate to the powder morphologies: small particle size favors high capacity values and the operation scan rate affects the capacity depending on the degree of crystallinity of the powder. On other hand, the battery capacity retention is better with microsized powders.

Keywords: Cu_3P; Morphology; Anode; Lithium ion battery; Size; Crystallinity

1. Introduction

Conceptually, electrode materials for Li-ion batteries have to show crystalline as well as electronic structures allowing the reversible intercalation of a large amount of lithium at a suited flat potential. Furthermore, low molecular weight and high molar density are required for greater specific and volumic capacities, as well as good electronic and Li^+ conductivities, especially at the solid–electrolyte interface. Technologically, electrode materials have to show a long and safe cycle life with limited, if any, morphological issues. Manufacturers are also concerned on the difficulty of preparing and handling the material. Some other characteristics remain more specific to each type of electrodes, anodes and cathodes. Refining these key parameters is the main objective for several research groups [1]. However, inside the battery, the reaction of lithium with the active material begins at the solid–liquid–electrolyte interface before any lithium diffuses through the material. How do the electronic and topological characteristics of the interface influence the electrochemical reactivity of the active material toward lithium? The morphology of electrode materials has become important with the development of new synthetic routes, such as ball-milling [2,3] and the observed corresponding enhancement of the electrochemical performances. An approach to answer this question is to prepare a single compound using methods leading to various powder morphologies, particle sizes and crystallinities, and then to compare the corresponding electrochemical behavior. Some work has been done in this field using a similar strategy [4,5]. The focus was however, more on the relationship between particle size and electrochemical reactivity rather than on the effect of powder morphology as a whole; particle size, surface state, and "bulk" crystallinity. Following our previous results on lithiated metal pnictides [6], nano to micro-structured first row transitional metal phosphides, with their easy preparation and good tuning of both particle size and crystallinity, have appeared as good candidates for the design of new anodes in the Li-ion battery. In this paper, we present our first results on copper phosphide, Cu_3P. Depending on the synthetic route, solvothermal [7,8], ball-milling, spray [9] or high temperature (or ceramic) [10], Cu_3P has shown various particle sizes and crystallinities. Electrochemical reactivity

☆ Supplementary data associated with this article can be found at doi: 10.1016/S0378-7753(04)00550-6.

* Corresponding author.
E-mail address: fredf@univ-montp2.fr (F. Favier).

0378-7753/$ – see front matter © 2004 Elsevier B.V. All rights reserved.
doi:10.1016/j.jpowsour.2004.05.024

towards lithium and electrode performances were evaluated in regards to the powder morphologies and crystallinities using galvanostatic and potentiodynamic measurements, electron microscopy, and X-ray diffraction (XRD).

2. Experimental

2.1. Reagents

Red phosphorus (99%, Aldrich), copper foil (Goodfellow, Cambridge Limited), copper powder metal (99.9%, Alfa Aesar), white phosphorus (old lab stock), $CuCl_2{\cdot}2H_2O$ (Prolabo), NH_4OH solution (35%, Fisher Chemicals), Ethylenediamine (99%, Acros Organics), polyoxyethylen glycol ether (Brij30), polyacrylamide carboxyl modified (MW 200,000, Aldrich), ethanol (anhydrous, Aldrich) were used as received, without any further purification.

2.2. Five different synthetic routes were used for the preparation of Cu_3P powders

Using the method described by Juza, Cu_3P was prepared at high temperature (HT) from stoichiometric amounts of metal copper and red phosphorus powders in sealed silica tube [10]. The temperature was increased to reach 600 °C or 900 °C using a ramp of 1 °C/min. The final temperature was then kept for 48 h. Finally, the samples were air cooled down. Ball-milling (BM) has recently been used as a powerful synthetic method for the preparation of electrode materials in Li-ion batteries [3]. BM syntheses were performed using a Spex 8000 mixer-mill. To prepare approximately 500 mg of Cu_3P, the stoichiometric amounts of precursor raw powders (Cu metal and red P) were placed into a stainless-steel container together with steel balls for a weight ratio of steel balls to powder in the range from 8:1 to 10:1. The grinding time for such a precursor mixture was set for 8 h for a complete reaction. The BM powders were annealed in sealed silica tubes at 900 °C (temperature ramp at 1 °C/min) under static vacuum for one week before being quenched in air. Annealed BM powders are referenced bellow as BMA.

For HT and BM syntheses, hygroscopic and O_2 sensitive reagents were stored and handled in a glove box filled with dry argon (oxygen contents below 5 ppm).

Thick films of Cu_3P (TF) were synthesized by solid state reaction at moderate temperature [9]. A red phosphorus suspension in ethanol was deposited by spray on a copper foil heated in air at 70 °C. By evaporation of the ethanol, a red film was produced over the copper foil. This supported film was fired at 400 °C for 10 h in flowing N_2. A black-grey film of Cu_3P was produced at the surface of the Cu foil.

A low-temperature synthesis of Cu_3P, was performed via a convenient solvothermal route (ST) [7]. A stainless-steel autoclave lined by Teflon was used for this preparation. Appropriate amounts of $CuCl_2{\cdot}2H_2O$ were dissolved in diluted NH_4OH, the resulting solution was mixed with pieces of white phosphorus in the Teflon vessel. The autoclave was tightly sealed and heated at 140 °C for 10 h. Safer red phosphorus can either be used in an alternative solvothermal route: a non-ionic water soluble polymer (polyacrylamide) or surfactant (polyoxyethylen glycol ether) was added to the mixture and diluted ammonia was replaced by ethylenediamine [8]. The reaction temperature was increased to 180–190 °C. Powders obtained by both methods were washed with H_2O and absolute alcohol, and dried overnight at 70 °C in vacuum. For such basic reaction media, the complex mechanism pathway includes the reduction of the copper chloride salt to small copper metal particles that react with phosphorus to lead to Cu_3P.

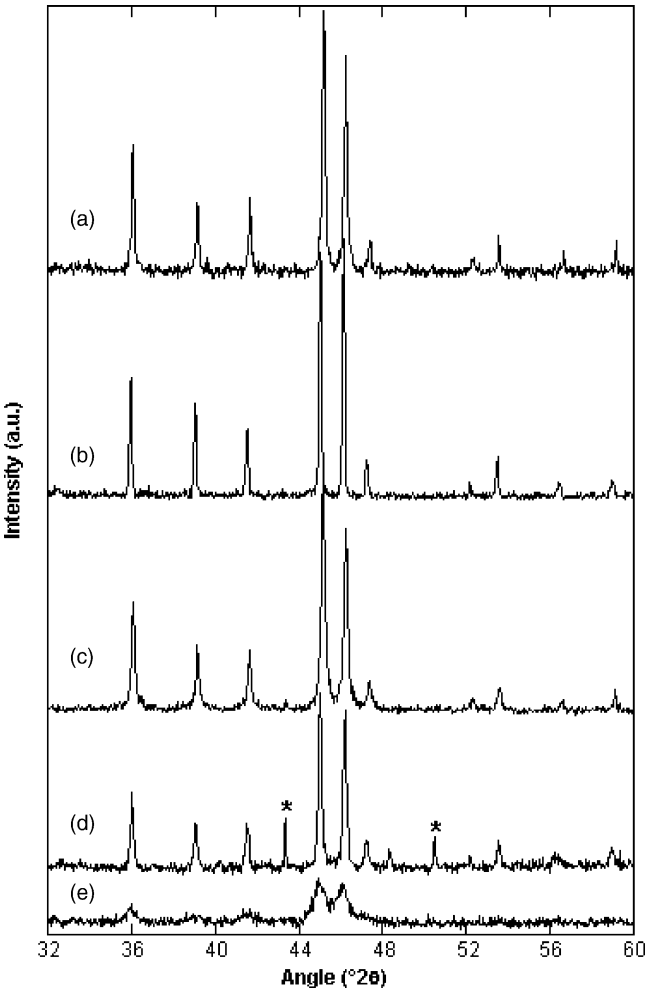

Fig. 1. X-ray diffraction patterns for Cu_3P powder prepared by HT (a), TFU (b), ST (c), BMA at 600 °C (d), BM (e). Copper metal peaks are identified by (*) mark in pattern (d).

Powder purities and crystallinities of prepared Cu_3P powders were checked by XRD (Fig. 1). Sampling was done in Lindeman capillaries and XRD patterns were recorded on a Philips X-pert diffractometer operating with a Cu $K\alpha_1$ radiation in the Debye–Scherrer geometry. The powder morphology was determined by scanning electron microscopy (SEM, JEOL 1200 EXII) on crude materials.

Electrochemical tests were performed in Swagelok^{TM}-type two-electrode cells assembled in an argon-filled dry box. These cells consisted of a composite electrode containing 10–12 mg of active material mixed with 15 wt.% of carbon black, a lithium metal disk as counter and reference electrode, and a Whattman GF/D borosilicate glass microfiber separator saturated with a 1 M $LiPF_6$ (ethylene carbonate:dimethylcarbonate, 1:1) electrolyte solution (Merck) placed in-between. The electrochemical insertion was monitored using a Mac Pile automatic cycling/data recording system (Biologic SA, Claix, France) operating in galvanostatic mode in the range 2–0.02 V. Using the same setup and equipment, potentiodynamic measurements have been done at a scan rate of 10 mV/h with a lower current limit corresponding to 1 Li/10 h.

TF were characterized by XRD and electrochemical measurements as unsupported powder obtained by smoothly scratching off Cu_3P layer (hereafter TFU powder). Electrochemical results for powders supported on Cu foil (TF) will not be discussed in the present paper since sampling (presence of a copper substrate, without any acetylene black addition) strongly differs to those used for other Cu_3P powders in the studied series and avoids any consistent comparison. Results on TF sample have been presented in a separate paper [9].

3. Results and discussion

XRD patterns reveal the crystallinity differences between Cu_3P powders obtained by the various routes explored during this study (Fig. 1). Two allotropic forms have been referenced for Cu_3P [10,11]: a high temperature form ($a = 4.09$ Å, $c = 7.19$ Å, P-3m1, $c/a = 1.76$, $Z = 2$), which crystallizes in an hexagonal sub-cell of the low-temperature form ($a = 6.97(5)$ Å, $c = 7.149(9)$ Å, P-3c1, $c/a = 1.025$, $Z = 6$). Despite the wide temperature range operated for the various synthetic routes, every Cu_3P phase prepared during this work was found to be low-temperature form. These patterns also confirm the purity of the prepared Cu_3P powders except for BMA powder (Fig. 1d) which is polluted by Cu metal impurities (less than 3 mol% as determined by Rietveld quantitative analysis). The XRD pattern for Cu supported Cu_3P (TF) shows some extra peaks from the copper substrate underneath the thick film (see Section 5). In contrast, the corresponding XRD pattern (Fig. 1b) confirms the chemical homogeneity of TFU powder.

By comparison of the averaged particle sizes for ST powders (TEM or SEM diameter ≈150 nm, Fig. 2c) and BM powders (SEM size ≈3 μm, Fig. 2a), the lack of crystallinity of the BM powders actually arises from crystal defects rather than from size effects. The structural distortions induced by the BM process mainly contribute to the increase of the full-width at half-maximum (FWHM) of the diffraction lines from ST to BM powders: nicely crystallized nanoparticles are obtained by ST method (Fig. 1c) while microsized amorphous powders are obtained by BM method (Fig. 1e). As expected, HT route led to highly crystallized bulk material (SEM size ≥50 μm, Fig. 2d) while, as shown Fig. 1d, annealing of BM powders at 600 °C greatly improved the crystallinity by erasing crystal defects for a limited increase of the particle size (SEM size ≈5 μm, Fig. 2b). Morphological differences, especially surface defects, between BM and BMA powders are more obvious on micrographies (Fig. 2a and b). TFU powders show morphological parameters, particle size as well as crystallinity, very close to those of ST powder (SEM size ≈200 nm, Fig. 2e). These small nanocrystallites are mostly aggregated to form larger grains (in average of 50 μm in size). An SEM imaging of TF sample surface (see Section 5) confirms the porous morphology of the prepared thick film. Note that any morphological differences could be evidenced between surfactant-assisted and surfactant-free ST powders neither by XRD nor by electronic microscopies (data not shown). The various synthetic routes range Cu_3P particle sizes almost over three orders of magnitude (from 150 nm to roughly 50 μm) while powder crystallinity varied from “defect-rich” X-ray amorphous powders to highly crystallized samples.

Whatever the synthetic methods and scan rates, galvanostatic curves roughly show similar features for the whole series, those are characteristic of a complex Li-insertion/extraction mechanism. The galvanostatic response for BMA powder at two different scan rates (1 Li/2 h and 1 Li/20 h) are given as examples Fig. 3. An in situ X-ray diffraction experiment done on ST powder reveals the discharge mechanism to proceed by insertion of Li inducing the sequential formation of $Li_xCu_{3-x}P$ phases by both solid solution processes and two-phase structural changes [12]. During this discharge, as Li electrochemically reacts with the powders, Cu(I) is progressively reduced to Cu(0). During the charge, as Li is progressively extracted from a Li-rich copper phosphide amorphous phase, copper metal is partially re-oxidized. At the end of charge, Cu_3P diffraction lines are recovered along with those of Cu. The next discharge follows the same pathway as the first one. This (partial) reversibility of the mechanism suggest Cu^+ to be reduced as small copper metal particles reactive enough to give some Cu_3P back. Such a process involving the reversible reduction of the metal to give metallic nanodomains has already been observed for the lithium reaction with 3-d transitional metal oxides (M = Co, Ni, Cu, Fe) [13] as well as in InSb system [14]. Anyway, considering the stoichiometry of the prepared copper phosphide, only three Li are expected to react with Cu_3P to give by full electrochemical conversion, Li_3P at the end of discharge. Up to 4.5–5 Li have however been reversibly exchanged especially with ST powder for a battery running at low scan rate. We have not so far reached any univocal and definitive explanation for this excess of inserted charges into the Cu_3P electrode but such a mishandling of the formal electron count has already been observed for lithium metal phosphide ternary phases [6]. On the other hand, the high starting potential and the first few shoulders

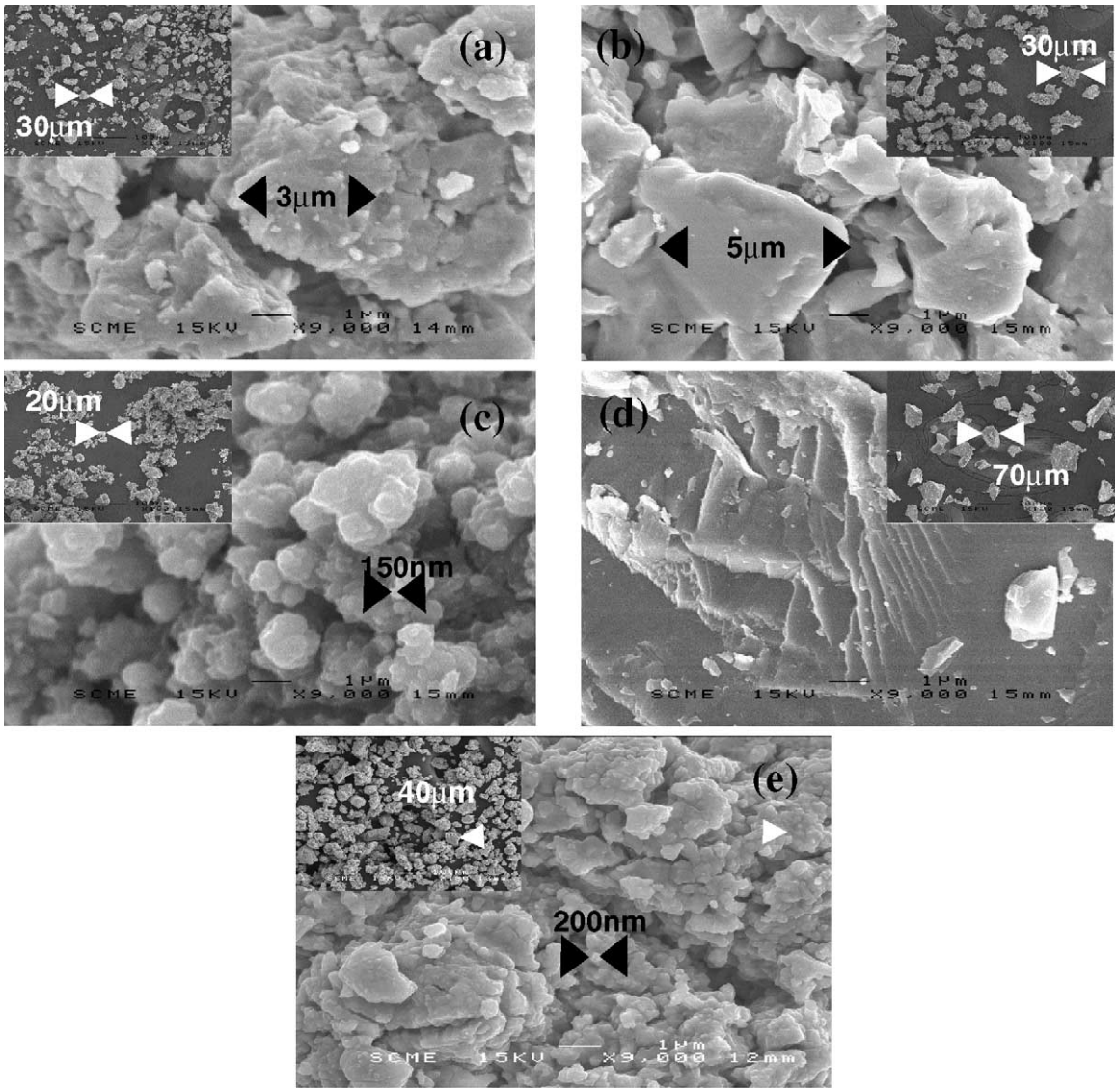

Fig. 2. SEM micrographies for Cu_3P powders prepared by (a) BM, (b) BMA, (c) ST, (d) HT, and (e) TFU. Inserts show the corresponding powder grain at lower magnification. Same magnifications have been used for the series.

in the galvanostatic curve, below $x = 0.6$ or 0.8, might as well account for electroactive impurities such as copper oxides [17]. Although X-ray diffraction does not show any extra diffraction lines from any impurities, this hypothesis will be discussed on the basis of potentiodynamic measurements in the next section.

A comparison of the ex situ X-ray diffraction patterns for as prepared HT Cu_3P and after a complete charge–discharge cycle (Fig. 4) shows (i) an increase in the FWHM of the diffraction peaks characteristic of the expected lower crystallinity of Cu_3P (45% of loss) produced back at the end of charge by such a solid state electrochemical process; (ii) a decrease in the diffraction peak areas at the end of charge characteristic of a loss of diffractive material (i.e. Cu_3P). From our experimental data, this disappearance of Cu_3P of about 9.9% calculated from (1 1 2), (2 0 2), (2 1 1), (3 0 0), (1 1 3), and (2 1 2) peak areas can be compared to 12% of capacity loss between the first discharge and charge (from galvanostatic measurement). The same approach on ST powder gives a 45% of cristallinity loss, and a 38% loss of diffractive material for a 36% loss of capacity at the end of the first cycle (Beryllium was used as internal standard). These agreements demonstrate the partial irreversibility of the process arising from an incomplete conversion of Cu back to Cu_3P during the charge rather than from any electrochemical interfacial by-reactions involving the electrolyte and taking place at low potential as usually observed for anode materials in Li-ion batteries [13]. Thus, the loss of capacity after the first reduction is definitively related to a composition change in the electrode during the oxidation rather than to some irreversible structural or textural changes [15]. Copper which is not completely converted back to Cu_3P at the end of charge does not react with Li and only the remaining part of Cu_3P is available for Li insertion for the next cycles.

Table 1
Capacity values at sweep #*n* for the various Cu_3P powders for two different scan regimes

	Capacity at first sweep (mAh/g)	Capacity at second sweep (mAh/g)	Capacity loss (%)	Capacity at sweep #*n*, *n* in parentheses (mAh/g)
1 Li/2 h				
HT	272	208	24	32 (84)
BM	359	240	33	235 (22)
BMA	298	184	38	19 (100)
ST	527	447	15	29 (100)
TFU	357	240	33	144 (43)
1 Li/20 h				
HT	413/+52%	392	5	284 (21)
BM	412/+15%	301	25	273 (39)
BMA	460/+54%	332	28	47 (40)
ST	615/+17%	472	23	71 (31)
TFU	670/+88%	352	47	53 (38)

Capacity loss corresponds to the loss in capacity between the first and second sweep. Along with initial capacity values at 1 Li/20 h scan rate, the value increase from 1 Li/2 h to 1 Li/20 h is given in percentage.

The main difference in the various galvanostatic curves lies in the corresponding specific capacity values (Table 1). The initial capacity value is higher with electrodes from ST or TFU powders than from BM or HT powders. This ranking has been roughly kept for both scan rates used in the present study. The measured particle size ranks the same way in the series. As a first conclusion, for both scan rates and without any reference to the powder crystallinity, the smaller the particle size, the higher the initial capacity. However, since annealing of BM powder has a limited impact on particle size, the slight increase of the initial capacity from BM to BMA microsized powder can definitively be associated to crystallinity effects. Particle size is a known issue on the Li diffusion at the electrolyte–solid interface [3–5] and structural long-range order could influence the Li diffusion mechanism within the structure [16]. Schematically, in the present case, crystallized Cu_3P nanoparticles favors high initial capacity while amorphous microsized particles are less favorable. As usually observed for electrode material in Li-ion batteries, scan rate affects the electrochemical performances of our Cu_3P anodes: the slower the scan rate, the higher the initial capacity. Moreover, by comparison of the initial capacities at both scan rates in the series, some morphological effects can be associated to the observed increase: from low to high scan rate, the initial capacity decreases for HT, BMA and TFU powders by at least 50% (up to 88% for TFU powder) while for BM and ST powders the corresponding increase is limited to about 15%. The last two powders are shown to present a lower crystallinity in

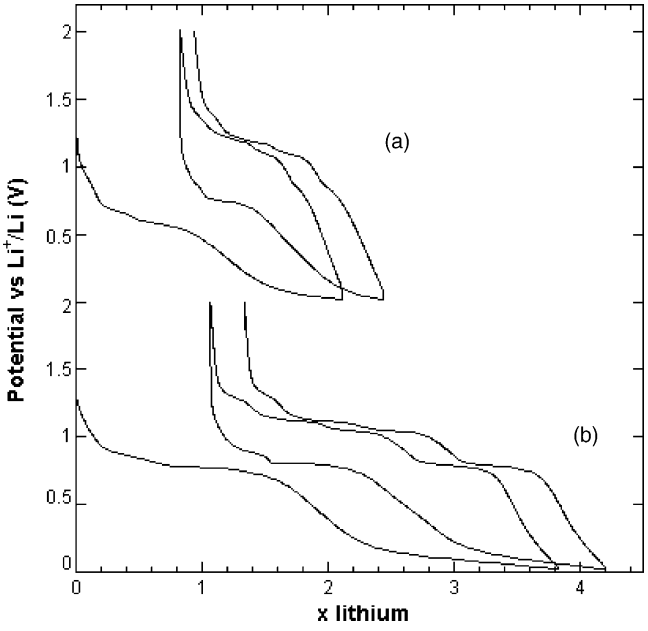

Fig. 3. Galvanostatic curves for Cu_3P prepared by BMA and operated at (a) 1 Li/2 h and (b) 1 Li/20 h scan rates. For the sake of clarity only the first two cycles are depicted.

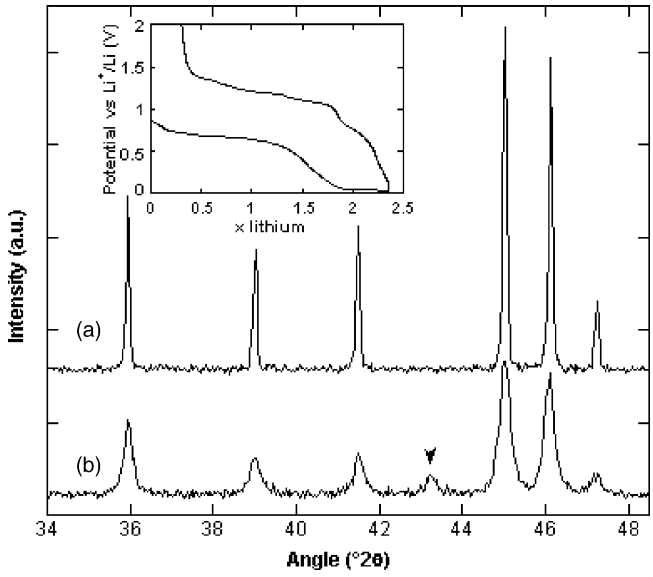

Fig. 4. XRD patterns of Cu_3P HT powder (a) as prepared and (b) after a complete discharge–charge cycle. The corresponding galvanostatic curve at 1 Li/2 h scan rate is given as insert. Copper (1 0 0) diffraction line is marked with an arrow head.

the series. Scan rate is more effective on crystallized rather on amorphous Cu_3P powders. This point is even more obviously demonstrated by comparison of the first capacity increase of +15% for BM powder which is up to +54% for BMA powder when scan rate is slowed down from 1 Li/2 h to 1 Li/20 h.

Depending on the synthetic route and scan rate, various losses in capacity are observed from first to second sweep (Table 1): the loss of electroactive material responsible for this capacity loss strongly depends on the powder morphology, especially the particle size. In the Cu_3P powder series, the smaller the particle size, the higher the capacity loss. As an attempt for an explanation, let's now focus on both extreme Cu_3P powder morphologies in the present study. For HT powder, as Li diffuses into the "large" microsized Cu_3P grain for a progressive conversion to $Li_xCu_{3-x}P$, Cu metal is generated as nano-inclusions into the bulk matrix. For micro and especially nanomaterials such as BMs, ST or TFU powders, copper metal is more presumably formed as individual nanoparticles at the surface or aggregated with the Li-rich nanophase. Matrix effects in the HT powder favors the charge reactivity to give Cu_3P back while "isolated" metal particles are obviously expected as being less reactive. For powders prepared by each synthetic route, the lower the scan rate, the lower the capacity loss. This effect is also correlated to the particle size: the scan rate is more effective on the capacity loss for small particle rather than for large particle. This latter point can be discussed on the basis of kinetic considerations. A comparison of BM and BMA capacity losses at both scan rates, respectively 33 and 36% at 1 Li/2 h, and 25 and 28% at 1 Li/20 h demonstrates the effect of powder crystallinity on the battery performances: for a given particle size, the lower the crystallinity, the lower the capacity loss at first cycle. The limited loss observed for the highly crystallized HT powder at both scan rates demonstrates the relative impact of crystallinity over particle size on the first capacity loss.

In contrast to galvanostatic curves, potentiodynamic curves marked some noticeable shape and peak position differences in the series. The potentiodynamic response of TFU powder is given as a representative example in Fig. 5. To confirm the reproducibility of the lithium insertion/extraction mechanism, the first two potentiodynamic cycles are depicted. As usually observed, peak definition improves after the first cycle. Further cycles do not show any differences. Anyway, this curve supports the complexity of this mechanism: four main peaks are observed in reduction at 0.90 V, 0.80 V, 0.26 V and 0.20 V respectively, the same number in oxidation at 0.77 V, 1.05 V, 1.11 V and 1.26 V respectively. Peak assignments have been extracted from potentiodynamic measurements done using various cut off potentials. The first reductive peak at 0.90 V (1) has thus been found to involve two distinct "events" as exhibited by its splitting at 1.11 V and 1.26 V in oxidation (1′). The intense and symmetric peak at 0.80 V (2) in reduction is characteristic of a two phase process and corresponds to the oxidation peak at 1.05 V (2′) while those at 0.26 V (3) and 0.20 V (4) in discharge are related to the broad and complex peak centered at 0.77 V (3′ and 4′) in charge. Potential values for the prepared Cu_3P powders are summarized Table 2.

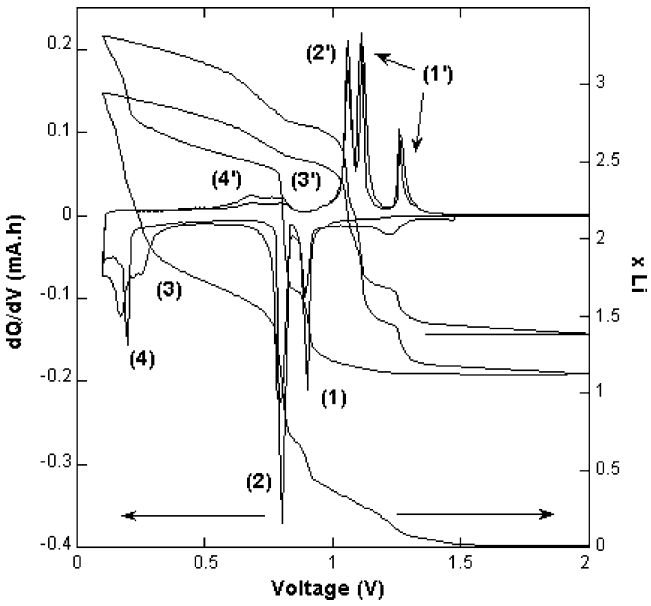

Fig. 5. Potentiodynamic response for TFU Cu_3P powder operated at 10 mV/h scan rate and current limit corresponding to 1 Li/10 h. Corresponding galvanostatic is given as a function of lithium content (x). Only the first two cycles are given.

Table 2
Potential values for potentiodynamic peak #n for the various Cu_3P powders (V vs. Li^+/Li)

	Reduction				Oxidation			
	#1[a]	#2	#3	#4	#4′ and #3′	#2′	#1′	
HT	0.90 (st,sym)	0.80 (st,sym)	–	0.20 (m,mul)	0.77 (br,w,mul)	1.05 (st,sym)	1.11 (st,sym)	1.26 (m,asym)
BM	0.89 (m,mul)	0.76 (st,sym)	0.46 (m)	0.12 (m,mul)	0.74 (st)	1.05 (st)	1.12 (st,asym)	–
BMA	0.88 (m,asym)	0.78 (st,sym)	0.45 (w,br)	0.13 (m,mul)	0.80 (br,w,mul)	1.06 (m,sym)	1.14 (m,sym)	1.32 (m,asym)
ST	0.90 (m,asym)	0.80 (st)	0.41 (w,br)	0.16 (m,mul)	0.77 (br,w,mul)	1.05 (st)	1.12 (st)	1.27 (m,asym)
TFU	0.90 (st,sym)	0.80 (st)	0.26 (m,br)	0.20 (m,mul)	0.77 (br,w,mul)	1.05 (st,sym)	1.11 (st,sym)	1.26 (m,asym)

Peak shape and intensity are given in parentheses as follows: st: strong, m: medium, w: weak, br: broad, sym: symmetric, asym: asymmetric, mul: convoluted peak. *Note*: Extra peaks at first reduction at (i) 0.6 V (w,sym) for HT; (ii) at 1.25 V (w,br) for TFU; (iii) at 1.15 V (w,asym) and 1.39 (w,asym) for ST.

[a] Peak number.

Despite these observed differences, these curves are characteristic for a complex but unique mechanism occuring during the electrochemical reaction of Cu_3P with Li. The greatest differences are observed for BM powder, and in a lesser extent for BMA and ST powders. Noteworthy is the fact that these powders show worst crystallinities in the series. This latter point makes sense since the corresponding Li-insertion/extraction mechanism implies structural transitions as well as solid solution processes involving long-range order changes. The few extra (and irreversible) peaks, observed at the beginning of the first reduction at potentials above 1.10 V, are associated to physically or chemically absorbed surface contaminants "washed out" at the first reduction, rather than to any morphological issues. This is especially obvious for TFU and ST Cu_3P fine powders which are synthesized in air while HT, BM, and BMA powders are prepared and handled under controlled O_2-free and H_2O-free atmosphere. Copper oxides are among the expected impurities and are known to react with lithium in a potential range above 1.2 V [5,17]. The insertion of Li in such impurities can account for a part (presumably less than 0.6–0.8 Li) of the large first sweep capacity observed for ST and TFU powders.

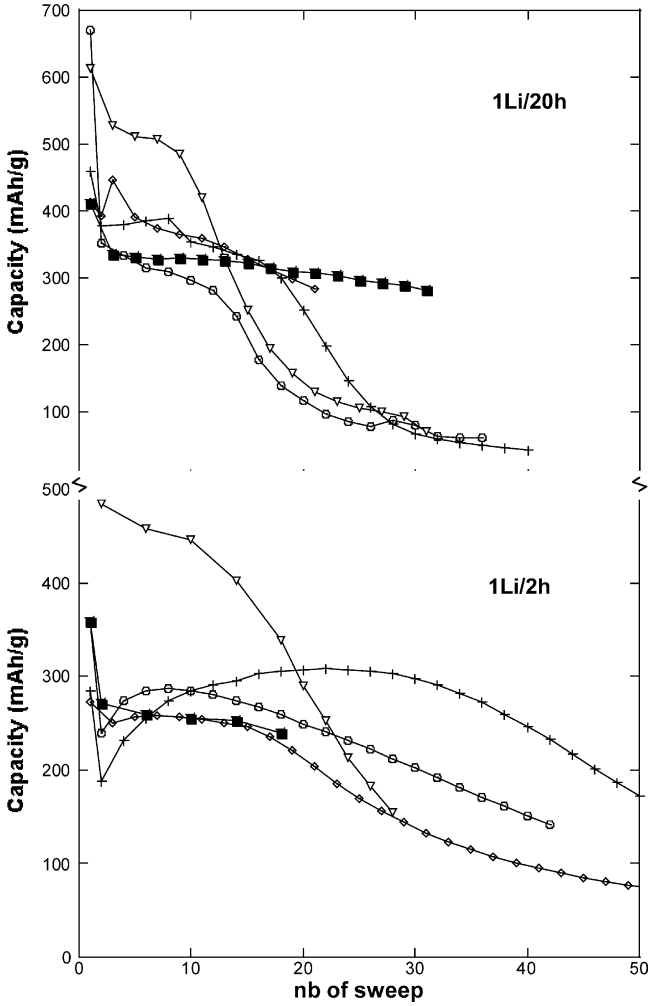

Fig. 6. Capacity as a function of the number of sweep for Cu_3P powder prepared by ST(▽), by BM (■), by HT (◇), by TFU (○), and by BMA (+). Capacity retention is depicted for both 1 Li/2 h and 1 Li/20 h scan rates.

Batteries built from the various Cu_3P powders were operated over several cycles (up to 50) to evaluate their capacity retention capabilities at two different scan rates. Fig. 6 shows the capacity of Cu_3P powders as a function of the number of sweep for 1 Li/2 h and 1 Li/20 h scan rates. For both scan rates, powders prepared by a single method have capacity evolving the same way. For example, ST powder capacities quickly reach a sloppy plateau over the first ten sweeps before to decrease down to low values. Moreover, HT curves remain almost "parallel" over twenty sweeps as do BM curves. Actually, for any prepared Cu_3P powders but those by ST method, capacity retentions roughly follow the same tendency. This capacity upon cycling does not at first seem to relate to any particular morphological aspects, particle size or crystallinity. BM as well as BMA Cu_3P powders however retain battery capacity on longer term. This latter point suggests microsized powder to promote a better capacity retention rather than nano structured or bulk material.

4. Conclusion

Although the presented results remain specific to Cu_3P electrochemical behavior toward lithium insertion/extraction, some "rules" may be pointed out for the formulation, preparation, and design of new anode materials for Li-ion batteries: nanostructured materials favor high initial capacity values and scan rate is then more effective on crystallized powder rather on amorphous powder. In contrast, capacity retention is uncorrelated to crystallinity, microsized powder however shows better results than nanostructured or bulk material. As usually observed, a compromise is certainly needed on the particle size and our works are now focused on thermal annealing of ST powders for the growth of Cu_3P nanocrystals in the nanometer to micrometer range.

5. Supplementary material

Galvanostatic (1 Li/2 h and 1 Li/20 h) as well as potentiodynamic curves are available for each prepared Cu_3P powders. SEM micrography and XRD pattern for TF sample.

Acknowledgements

This work is supported by the *Matériaux* funding program from the Centre National de la Recherche Scientifique (CNRS). H. Pfeiffer thanks the Région des Pays de la Loire, France, for financial support. Thanks to E. Walter from UC Irvine (USA) for helpful discussions.

References

[1] Lithium Batteries: Science and Technology, G.A. Nazri, G. Pistola (Eds.), Kluwer Academic Publishers, 2003.
[2] J.M. Tarascon, M. Armand, Nature 414 (6861) (2001) 359–367; K. Wang, J. Yang, J. Xie, B. Wang, Z. Wen, Electrochem. Comm. 5 (6) (2003) 480–483.
[3] F. Gillot, M.-P. Bichat, F. Favier, M. Morcrette, J.M. Tarascon, L. Monconduit, Ionics 9 (12) (2003) 71.
[4] H. Mukaido, A. Yoshizawa, T. Momma, T. Osaka, J. Power Sources 60–63 (119–121) (2003) 10–22.
[5] S. Grugeon, S. Laruelle, R. Herrera-Urbina, L. Dupont, P. Poizot, J.M. Tarascon, J. Electrochem. Soc. 148 (4) (2001) 285.
[6] M.-L. Doublet, F. Lemoigno, F. Gillot, L. Monconduit, Chem. Mater. 14 (2002) 4126.
[7] H.L. Su, Y. Xie, B. Li, X.M. Liu, Y.T. Qian, Solid State Ionics 122 (1–4) (1999) 157–160.
[8] J. Liu, X. Chen, M. Shao, C. An, W. Yu, Y. Qian, J. Cryst. Growth 252 (1–3) (2003) 297–301.
[9] H. Pfeiffer, F. Tancret, M.-P. Bichat, L. Monconduit, F. Favier, T. Brousse, Electrochem. Comm. 6 (2004) 263–267.
[10] H. Schlenger, H. Jacobs, R. Juza, Z. Anorg. Allg. Chemie Bd385 (1971) 177–201.
[11] O. Olofson, Acta Chem. Scand. 26 (1972) 2777–2787.
[12] M.-P. Bichat, T. Politova, L. Monconduit, J.L. Pascal, F. Favier, J. Electrochem. Soc., in press.
[13] F. Badway, I. Plitz, S. Grugeon, S. Laruelle, M. Dolle, A.S. Godz, J.M. Tarascon, Electrochem. Solid-State Lett. 5 (2002) 6.
[14] J.T. Vaughey, K.D. Kepler, R. Benedek, M.M. Thackeray, Electrochem. Commun. 1 (1999) 517.
[15] E. Peled, J. Electrochem. Soc. 126 (1979) 2047.
[16] M. Doyle, J.P. Meyers, J. Newman, J. Electrochem. Soc. 147 (1) (2000) 99.
[17] A. Débart, L. Dupont, P. Poizot, J.B. Leriche, J.M. Tarascon, J. Electrochem. Soc. 148 (11) (2001) 1266.